Nano Today 34 (2020) 100955

Contents lists available at ScienceDirect

Nano Today

journal homepage: www.elsevier.com/locate/nanotoday

Insights into the electronic origin of enhancing the catalytic activity of Co_3O_4 for oxygen evolution by single atom ruthenium

Changtai Zhao[a,b,1], Yan Tang[c,1], Chang Yu[a], Xinyi Tan[a], Mohammad Norouzi Banis[b], Shaofeng Li[e], Gang Wan[e], Huawei Huang[a], Lei Zhang[b], Huaixin Yang[d], Jun Li[c,**], Xueliang Sun[b,**], Jieshan Qiu[a,f,*]

[a] State Key Lab of Fine Chemicals, School of Chemical Engineering, Liaoning Key Lab for Energy Materials and Chemical Engineering, School of Chemical Engineering, Dalian University of Technology, Dalian, 116024, China
[b] Department of Mechanical and Materials Engineering, University of Western Ontario, London, ON, N6A 5B9, Canada
[c] Department of Chemistry and Key Laboratory of Organic Optoelectronics & Molecular Engineering of Ministry of Education, Tsinghua University, Beijing, 100084, China
[d] Beijing National Laboratory for Condensed Matter Physics, Institute of Physics, Chinese Academy of Sciences, Beijing, 100190, China
[e] Stanford Synchrotron Radiation Lightsource, SLAC National Accelerator Laboratory, Menlo Park, CA, 94025, United States
[f] College of Chemical Engineering, Beijing University of Chemical Technology, Beijing, 100029, China

ARTICLE INFO

Article history:
Received 23 May 2020
Received in revised form 25 July 2020
Accepted 16 August 2020
Available online 30 August 2020

Keywords:
Single-atom catalyst
Oxygen evolution reaction
Co_3O_4
Electronic structure
Catalytic activity

ABSTRACT

The surface electronic structure of transition-metal oxide catalysts plays a decisive role in binding the intermediates of the oxygen evolution reaction (OER) to the oxide surface, in turn influencing the catalytic activity of these materials. However, the approaches to modulating the electronic structure of surface metal ions are rare and far behind the demands. Here, we report a surface single atom decoration for adjusting the surface electronic structure of Co_3O_4, leading to enhanced electrocatalytic activity for OER, in which the isolated Ru single atoms were uniformly deposited on the surface of Co_3O_4 by an atomic layer deposition technology. As the OER catalyst, the as-made catalysts have exhibited a significantly enhanced catalytic activity (with increasing to 95.5 times) and a dramatically decreased overpotential. The density functional theory calculations reveal that the single-atom Ru acts as a promotor to adjust the 3d electronic structure of adjacent Co atoms and to tune the binding energy between intermediates and activity sites, finally leading to enhanced catalytic activity.

Contents

* Corresponding author at: State Key Lab of Fine Chemicals, School of Chemical Engineering, Liaoning Key Lab for Energy Materials and Chemical Engineering, School of Chemical Engineering, Dalian University of Technology, Dalian, 116024, China.
** Corresponding authors.
E-mail addresses: junli@tsinghua.edu.cn (J. Li), xsun9@uwo.ca (X. Sun), jqiu@dlut.edu.cn (J. Qiu).
[1] The first two authors contributed equally to this work.

https://doi.org/10.1016/j.nantod.2020.100955
1748-0132/

Introduction

Electrochemical water splitting is one of the most promising approaches to storing and utilizing renewable energy resources in the form of clean chemicals [1,2]. In spite of its significance, there is still a key challenge in the design of efficient yet cheap catalysts to accelerate the sluggish oxygen evolution reaction (OER), which is induced by a complex four proton-coupled electron transfers process [3–5]. Noble metal oxides of RuO_2 and IrO_2 demonstrated the excellent catalytic activity. However, their wider applications are restricted by the high price and poor stability [6,7]. Thus, it is indispensable to develop the cheap, earth-abundant, highly active, and durable catalysts for replacing the noble metal-based catalysts.

First-row transition metal-based catalysts, for instance, Co_3O_4, representing a new type of effective catalysts as possible alternatives to noble metal-based catalysts, recently have sparked worldwide research interests owing to the advantages in terms of low cost, abundant reserves, and good durability [8–11]. However, they underperform relative to the state-of-the-art OER catalysts. To enhance the electrocatalytic activity of this kind of catalysts can provide exciting opportunities for the development of OER. Except for the efforts to design unique nanostructures for increasing the amount of exposed active sites [12–16], modifying the electronic structure of catalysts is another strategy to systematically improve the intrinsic OER activity [17–20]. This is because 3d orbital electronic configuration plays a decisive role in the influence of binding energy of OER intermediates (*OH, *O, and *OOH) on the oxide surface, thereby OER activity [5,21–23].

Bockris and Otagawa reported that OER activities of transition metal-based catalysts are related to the 3d orbital electron number of the surface transition metal ions [24]. Yang et al. demonstrated that the activities of transition metal oxide catalysts depend on the occupancy of the 3d electron with an e_g symmetry of surface transition metal ions. The near-optimal OER catalysts feature the e_g occupancy close to unity [25]. In light of these theories, Sargent et al. proposed the use of tungsten to modulate the 3d electronic structure of metal oxides that can significantly enhance the electrocatalytic activity [26]. Nevertheless, the approaches that can finely regulate the electronic structure of surface metal ions are rare and highly demanded.

Single-atom catalysts have become the most active frontier in various chemical reactions and exhibit distinctive performances due to their nearly 100 % atom utilization efficiency, unique local coordination environment, and electronic configuration [27–29]. In most reactions, single-atom catalysts act as active centers, and the local coordination atoms play the role in tuning the electronic structure of single-atom catalysts [30–33]. In other words, single-atom sites also influence the electronic structure and catalytic behaviors of adjacent atoms. Bao et al. reported a strategy of single-atom Pt doping to trigger the catalytic activity of inert two-dimensional MoS_2 surface [34]. Coincidentally, Xing et al. reported an atomic palladium interfacial doping to chemically activating the hydrogen evolution activity of inert MoS_2 [35]. Besides, Zhang et al. proposed an electrocatalyst of single-atom Au supported on NiFe LDH for OER. In this hybrid catalyst, Au is not an active site, but it can effectively modify the adsorption energies of OER intermediates on active sites, thus leading to a high OER activity [36]. Thus far, little has been done on surface single atom engineering to adjust the electronic structure of transition metal oxide catalysts for enhancing the OER catalytic activity, in which the electronic origin of catalytic activity enhancement needs to be clarified.

Herein, we developed a single-atom doping approach to modulating the surface electronic configuration of transition metal-based catalysts and enhancing the OER activity. In this study, an advanced atomic layer deposition (ALD) technology was employed to uniformly deposit isolated Ru single atoms on the surface of Co_3O_4 (Co_3O_4-Ru_1). Aberration-corrected high-angle annular dark-field scanning transmission electron microscopy (AC HAADF-STEM) and extended X-ray absorption fine structure (EXAFS) measurements confirmed the formation of isolated Ru single atoms. The density functional theory (DFT) calculations indicated that single-atom Ru plays a unique role in adjusting the electronic structure of adjacent Co atoms rather than as the active sites. The regulated 3d electronic configuration of adjacent Co atoms has altered the binding energy between intermediates and activity sites, leading to enhanced catalytic activity. Because of this, the overpotential of Co_3O_4 at 10 mA cm^{-2} decreases by 118 mV, and the catalyst activity increases to over 95.5 times due to the presence of Ru single atoms.

Experimental section

Materials preparation

Typically, 1.52 g of $CoCl{\cdot}6H_2O$ and 1.92 g urea were dissolved into 80 mL of water. Then, a piece of Ni foam (4 × 5.5 cm, washed with 1 M HCl and water) and the prepared solution were transferred into a Teflon-lined stainless-steel autoclave of 100 mL and kept at 95 °C for 8 h. After washing and drying, the precursor was annealing at 500 °C for 3 h with a ramp rate of 5 °C min^{-1}, yielding the composite.

Single-atom Ru was deposited on Co_3O_4 by ALD (Savannah100, Cambridge Nanotechnology Inc., USA) using bis(ethylcyclopentadienyl)ruthenium(II) and O_2 as precursors. High-purity N_2 (99.9995 %) was used as both purge gas and carrier gas. The free-standing material of Co_3O_4 grew on Ni foam was put in the ALD reactor chamber. The deposition temperature was 270 °C, and the container for bis(ethylcyclopentadienyl)ruthenium(II) was kept at 110 °C to provide a steady-state flux of Ru precursor to the reactor. Gas lines were held at 150 °C to avoid precursor condensation. For each ALD cycle, 1 s of the bis(ethylcyclopentadienyl)ruthenium(II) pulse and 5 s of the O_2 pulse were separated by a 20 s N_2 purge. The samples of Co_3O_4-Ru_1 and Co_3O_4-5Ru were prepared by conducting 2 and 5 ALD cycles, respectively. TiO_2-2Ru and TiO_2-5Ru were also prepared by conducting 2 and 5 ALD cycles, respectively.

Materials characterization

Morphology of the as-made catalyst was characterized by scanning electron microscopy (SEM, Hitachi S-4800), TEM (FEI TF30), and AC HAADF-STEM (JEOL JEM-ARM200 F). The X-ray diffraction (XRD) and X-ray photoelectron spectroscopy (XPS) measurements

were taken on a D/Max-III-type X-ray spectrometer with Cu Kα radiation (λ = 1.5406 Å) and Thermo ESCALAB 250, respectively. The X-ray absorption spectra (XAS) tests were performed in the Canadian Light Source.

Electrochemical measurements

The catalysts are free-standing electrodes without using any binder. The Co_3O_4-Com RuO_2 catalyst was prepared by dropping the RuO_2 dispersed solution with Nafion (Sigma Aldrich, 5 wt%) onto the Co_3O_4 electrode. The electrochemical measurements were performed in a standard three-electrode system on a CHI 760D electrochemical workstation using 1 M KOH as an electrolyte. Pt wire and Ag/AgCl were used as counter and reference electrodes, respectively. Before the electrochemical measurement, the electrolyte was degassed by bubbling oxygen for at least 30 min to ensure the saturation of the electrolyte. Linear sweep voltammetry (LSV) was recorded at a scan rate of 5 mV s^{-1} for the polarization curves. To achieve the best curve shape as well as avoid curve distortion by overcompensation, all polarization curves were corrected with an optimal iR-compensation level of 95 %. The electrochemical active surface area was evaluated by testing cyclic voltammograms in a potential range of 1.287–1.337 V vs. RHE, with scan rates of 1, 2, 5, 8, and 10 mV s^{-1}. Electrical impedance spectroscopy (EIS) measurements were carried out in the same configuration at 1.55 V and 1.60 V vs. RHE from 10^5 to 1 Hz and with an amplitude of 5 mV. Chronopotentiometric measurements were recorded under the same experimental system without iR-compensation via applying a current density of 10 mA cm^{-2} on working electrode for 100 h. All the electrochemical measurements were carried out at room temperature.

The turnover frequency (TOF) value is calculated from the equation:

$$TOF = j * S/(4F * n)$$

Here, j (A cm^{-2}) is the measured current density at a given overpotential, S is the surface area of electrode (cm^{-2}), the number 4 means 4 electrons per mole of O_2, F is Faraday's constant (96485.3 C mol^{-1}), and n is the mole number of the active metal sites for the catalysts that are deposited on the electrode.

Computational parameters and models

All the calculations were performed by periodic DFT with the Vienna Ab-initio Simulation Package [37,38]. Projector augmented wave method was used to describe the interaction between the atomic cores and electrons. The valence orbitals of Co (3d, 4 s), Ru (4d, 5 s), O (2 s, 2p) and H (1 s) were described by plane-wave basis sets with cutoff energies of 400 eV [39]. The exchange-correlation energies were calculated by generalized gradient approximation with the Perdew-Burke-Ernzerhof (PBE) functional [40]. Spin polarization was considered using unrestricted Kohn-Sham formalism. To correct the strong electron-correlation properties of these oxides, coulomb repulsion correction term of U within the Hubbard scheme (PBE + U) was applied in the 3d electrons of Co [41,42]. The effective U_{eff} value was set to 3.5 eV, which is used to investigate electrocatalytic oxygen evolution activity on cobalt oxides in previous computational work [43]. Co_3O_4 (001) surface was modeled as periodic slabs with eight Co layers in a (1 × 1) supercell, and the vacuum gap was ~15 Å. The k-point sampling consists of 3 × 3 × 1 Monkhorst − Pack points. The bottom four layers were fixed and the other atoms were fully optimized until the residual force on each ion was less than 0.02 eV/Å. After the optimization, the magnetic moments of Co^{2+} ions at tetrahedral sites are ~2.6 μB, and the Co^{3+} ions at octahedral sites are nonmagnetic except the surface Co^{3+} ions (~2.0 μB).

Free energy profile in OER

To calculate the free energy reaction profile of OER, we first obtain the enthalpy energy of each elementary step (ΔH at 0 K, 0 bar), which approximatively equals to the DFT total energy (ΔE) after ZPE correction (ΔE_{ZPE}). For adsorbed species, ΔH at 0 K, 0 bar is a good approximation to the Gibbs free energy (ΔG), since the entropy (S) contributions are small. However, for gaseous or liquid molecules, such as oxygen, hydrogen, and water, we cannot ignore the large entropy term at elevated temperatures. Therefore, the G of H_2O and H_2 can be estimated by the equation:

$$G = E + E_{ZPE} + H(0 \rightarrow 298K) - T \times S$$

where E_{ZPE}, H (0→298 K) and S are the ZPE correction, enthalpy difference between 0 K and 298 K, and entropy, respectively.

The G of O_2 (derived as $G[O_2]$) can be calculated with the equation according to the OER equilibrium at the standard conditions:

$$G[O_2] = 4.92eV + 2G[H_2O] - 2G[H_2]$$

Next, we must consider the proton when calculating the Gibbs free energy change (ΔG) of an elementary step. It is well-known that when pH = 0 in the electrolyte and 1 bar of H_2 in the gas phase at 298 K, the reaction free energy of $1/2H_2 \rightarrow H^+ + e^-$ equals to zero at an electrode potential of U = 0. Therefore, at standard conditions (U = 0, pH = 0, p = 1 bar, T = 298 K), ΔG of the reaction $^*AH \rightarrow A + H^+ + e^-$ equals to ΔG of the reaction $^*AH \rightarrow A + 1/2H_2$. Finally, the effect of a bias on all states involving an electron in the electrode should be corrected, by shifting the energy of this state by $\Delta G_U = -eU$, where U is the electrode potential relative to the standard hydrogen electrode. The potential determining step (pds) is the highest free energy step in the OER process, which is also the last step to become downhill in free energy when the potential increases. With this approach, the theoretical overpotential (η) at standard condition is defined as:

$$\eta = (G_{pds}/e) - 1.23V$$

Results and discussion

The schematic process for the synthesis of single-atom Ru on Co_3O_4 by ALD is shown in Fig. 1a. The Ru precursor of (Bis(ethylcyclopentadienyl)ruthenium(II)) as the first chemical species reacted with the Co_3O_4 substrate. The O_2 gas as the second species was used to take away the organic functional groups from the Ru precursor. The chemical bonding between the Ru precursor and Co_3O_4 enables a strong interaction between the deposited material and support and allows the homogeneous dispersion of Ru atoms [44].

The morphology of as-prepared catalyst was investigated by SEM and TEM. As shown in Fig. S1 and S2, the as-prepared catalyst features a typical nanowire-shaped structure, and there are no Ru nanoparticles on the surface. AC HAADF-STEM measurement was carried out to observe the catalyst at atomic resolution. As shown in Fig. 1b, some bright spots are uniformly distributed on Co_3O_4 substrate. The magnified STEM image shows that the Ru element is dispersed on Co_3O_4 surface as isolated single atoms, beyond which no Ru nanoclusters and nanoparticles (Fig. 1c). As shown in Fig. S3, the energy-dispersive X-ray spectroscopy (EDX) spectrum of Co_3O_4-Ru_1 shows the characteristic peaks of Co, Ru, and O elements, confirming the presence of Ru element, but the Ru peak

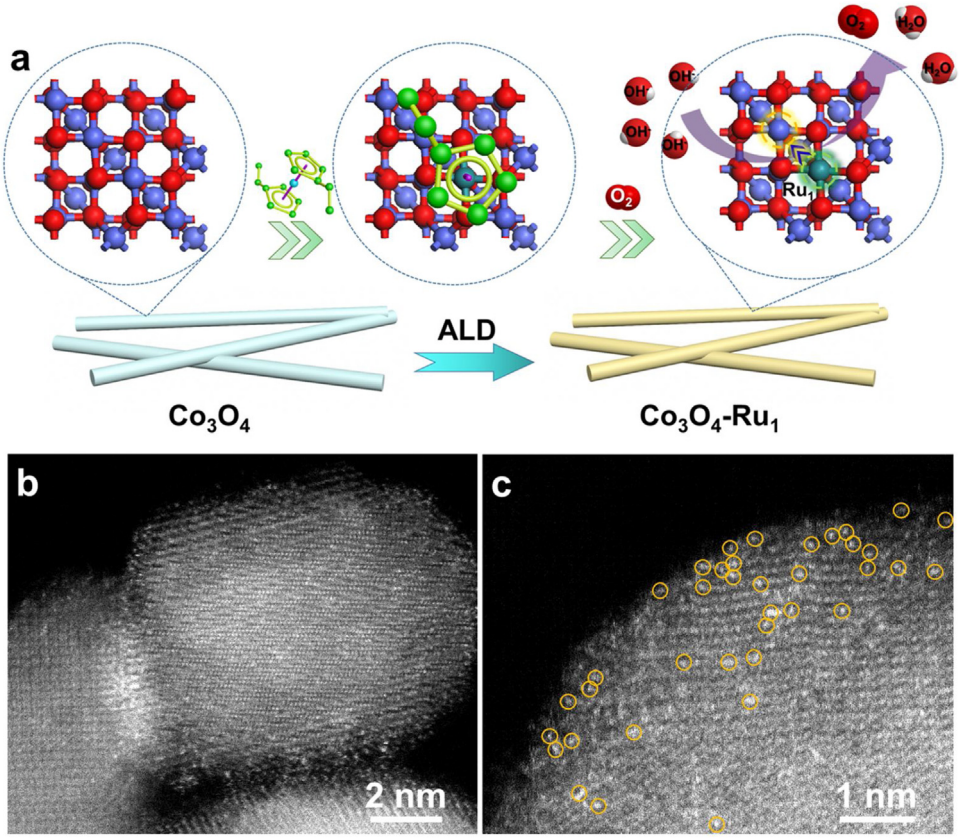

Fig. 1. Schematic ALD process and morphology characterizations of Co_3O_4-Ru_1. (a) Schematic illustration for the synthesis of single-atom Ru on Co_3O_4 by ALD and the catalytic process of Co_3O_4-Ru_1 for OER. (b-c) AC HAADF-STEM images of Co_3O_4-Ru_1.

features a weak intensity, suggesting a low loading. The XRD pattern of Co_3O_4-Ru_1 does not present any characteristic peaks of Ru or RuO_2 (Fig. S4). The content of Ru is determined to be approximately 1.61 wt% according to inductively coupled plasma optical emission spectrometry analysis (Table S1). The composite with 5 cycles ALD (named as Co_3O_4-5Ru) was also prepared. As shown in Fig. S5, there are some Ru clusters and many isolated Ru single atoms on the Co_3O_4-5Ru sample. The content of Ru increases to 3.98 wt%.

In order to further confirm the presence of single-atom Ru and study their chemical states and local coordination environment, XAS measurements were conducted. Fig. 2a shows the X-ray absorption near-edge structure (XANES) spectra of Ru K-edge of Co_3O_4-Ru_1, Ru foil, and RuO_2. It can be noted that the Ru K-edge absorption edge of Co_3O_4-Ru_1 is located in-between that of Ru foil and RuO_2, indicating that the valence of Ru in this catalyst is situated in between Ru^0 and Ru^{4+}. This also suggests that single-atom Ru features a strong interaction with the Co_3O_4 substrate and has an influence on the local electron environment [36]. Fourier transformed (FT) k_3-weighted EXAFS spectra of Co_3O_4-Ru_1, Ru foil, and RuO_2 are shown in Fig. 2b. The catalyst of Co_3O_4-Ru_1 presents two prominent peaks at 1.6 Å and 2.6 Å, which are assigned to the Ru-O and Ru-Co bonds, respectively [45]. As shown in Fig. 2c, d, and S6 and Table S2, the fitting data with Ru-Co bond show better matching than the fitting data with Ru-Ru bond, further confirming the formation of single-atom Ru and the Ru-Co bond. These results demonstrate the atomic dispersed Ru and the bonding form of isolated single-atom Ru. The catalyst of Co_3O_4-5Ru was also studied by XAS measurements. As shown in Fig. S7, the Co_3O_4-5Ru shows similar chemical valence and coordination environment to Co_3O_4-Ru_1 due to the fact that single-atom Ru is the main existing form of Ru element in Co_3O_4-5Ru. As shown in Fig. S8, there is no obvious difference in Co XPS spectra of Co_3O_4 and Co_3O_4-Ru_1. This is due to that the decoration of Ru single atoms is just on the surface of Co_3O_4, and the ratio of Co to Ru is as high as 78.2. Thus, most of Co atoms keep their original chemical states.

The electrocatalytic activity of Co_3O_4-Ru_1 for OER in 1 M KOH solution was evaluated by LSV at a scan rate of 5 mV s^{-1} with *iR* correction. For comparison, the reference catalysts of pure Co_3O_4, as well as Co_3O_4 with commercial RuO_2 (0.29 mg cm^{-2}) (Co_3O_4-Com RuO_2), were also tested under the same conditions. The oxidation peaks in Fig. 3a correspond to the formation of Ni (III) or Ni (IV) species, which are catalytically active for OER. As shown in Fig. 3a, the catalyst of Co_3O_4-Ru_1 shows the lowest onset potential of 1.42 V, which is *ca.* 70 and 105 mV ahead of the Co_3O_4-Com RuO_2 and Co_3O_4, respectively, indicative of its remarkable catalytic activity. Subsequently, it exhibits the highest current density at the same overpotential than the pure Co_3O_4 and Co_3O_4-Com RuO_2. Notably, it just needs an overpotential of 249 mV to drive the current density of 10 mA cm^{-2} on Co_3O_4-Ru_1, which is much lower than the 367 mV and 345 mV of Co_3O_4 and Co_3O_4-Com RuO_2, respectively (Fig. 3b). In other words, a large potential of 118 mV is decreased after depositing Ru single atoms, indicating that the catalytic activity is significantly enhanced and superior to the commercial catalyst. Even at a current density of 50 mA cm^{-2}, the overpotential of Co_3O_4-Ru_1 is also just 321 mV (Fig. 3b). In order to further analyze the dramatic change of catalytic activity, the curve of deducting the contribution of pure Co_3O_4 was also obtained. The overpotential at 10 mA cm^{-2} is also just 264 mV, further highlighting the excellent catalytic activity of active sites. The high catalytic activity of Co_3O_4-Ru_1 can also be evidenced by the lower charge transfer resistance compared with the pure Co_3O_4 (Fig. S9). As shown in Fig. S10, the Tafel slopes of Co_3O_4, Co_3O_4-Com RuO_2, and Co_3O_4-Ru_1 are 82, 86, and 104 mV/decade, respectively. The Tafel slopes of Co_3O_4-Com

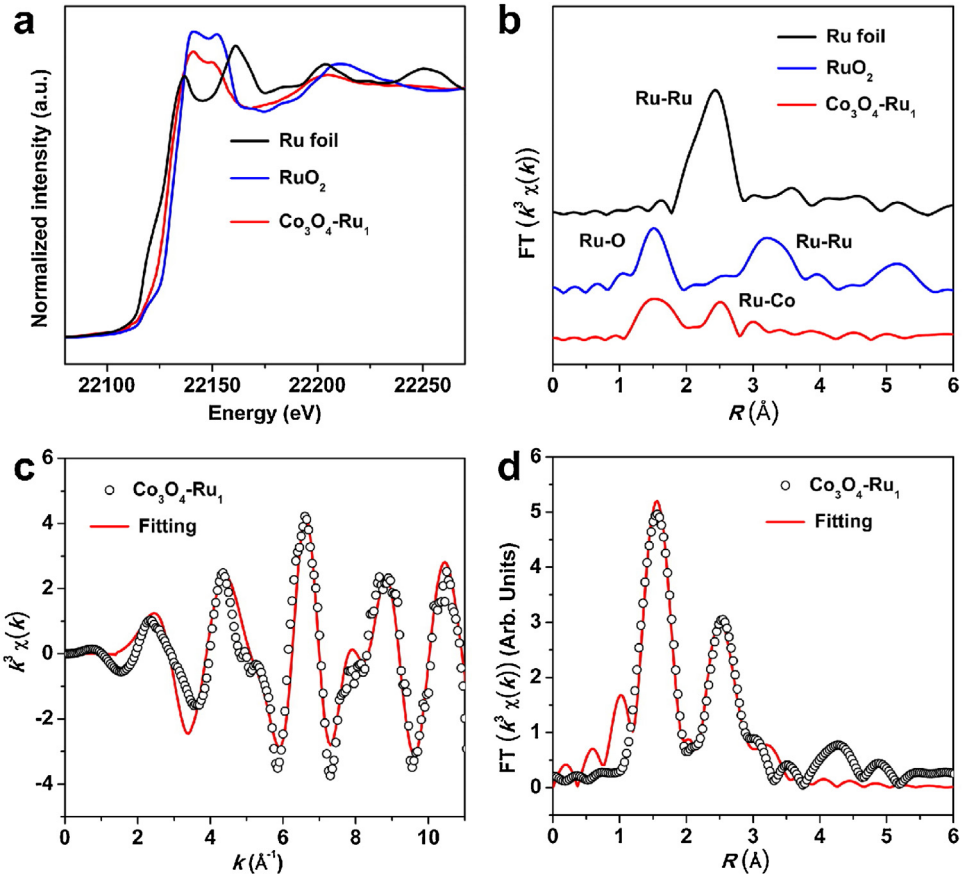

Fig. 2. XAS characterizations of the Co_3O_4-Ru_1. (a) Normalized XANES spectra and (b) EXAFS spectra of Ru foil, RuO_2, and Co_3O_4-Ru_1. EXAFS (c) k space and (b) R space spectra of Co_3O_4-Ru_1 and the fitting data.

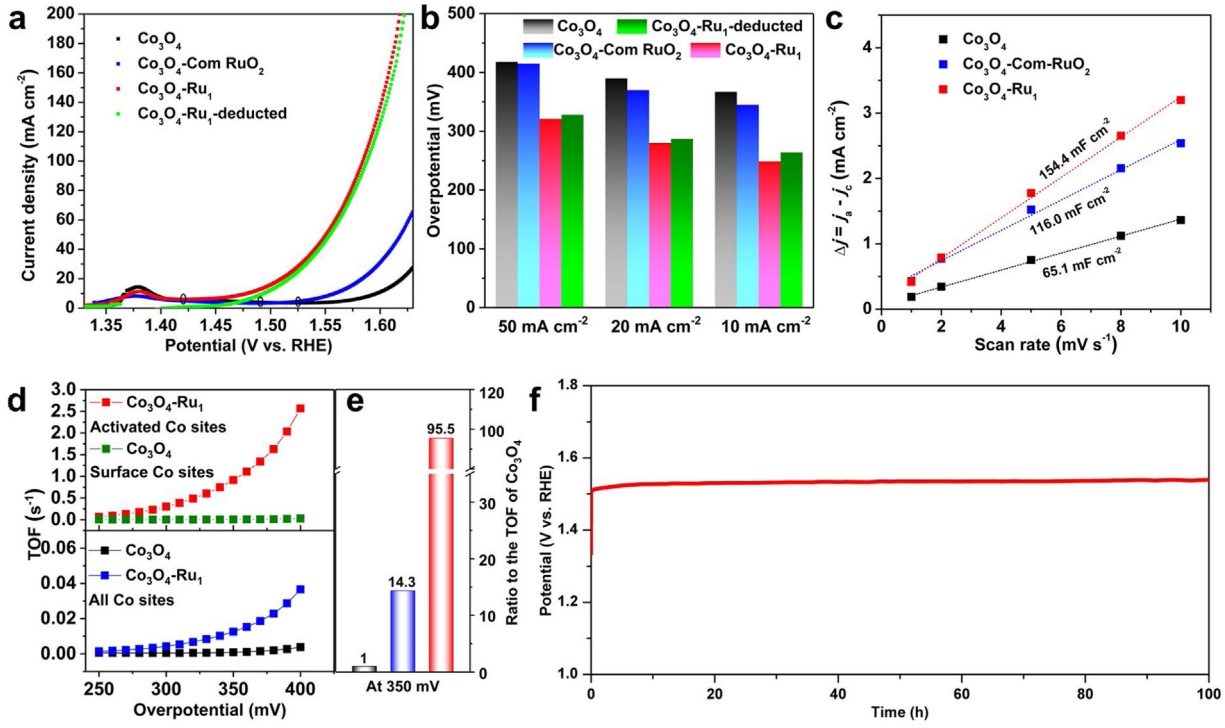

Fig. 3. Electrocatalytic performance. (a) The OER polarization curves of various catalysts at a scan rate of 5 mV s^{-1} with *iR* correction. (b) Overpotentials of various catalysts at different current densities obtained from OER polarization curves. (c) The electrochemical active surface area of various catalysts. (d) TOFs with respect to all Co atoms and surface Co atoms of Co_3O_4 and TOFs with respect to all Co atoms and activated Co atoms of Co_3O_4-Ru_1. (e) The ratio of TOFs with respect to different Co atoms to the TOF of Co_3O_4, all Co sites of Co_3O_4 to all Co sites of Co_3O_4 (black), all Co sites of Co_3O_4-Ru_1 to all Co sites of Co_3O_4 (blue), activated Co atoms of Co_3O_4-Ru_1 to surface Co sites of Co_3O_4 (red). (f) Long-term stability of Co_3O_4-Ru_1 at 10 mA cm^{-2}.

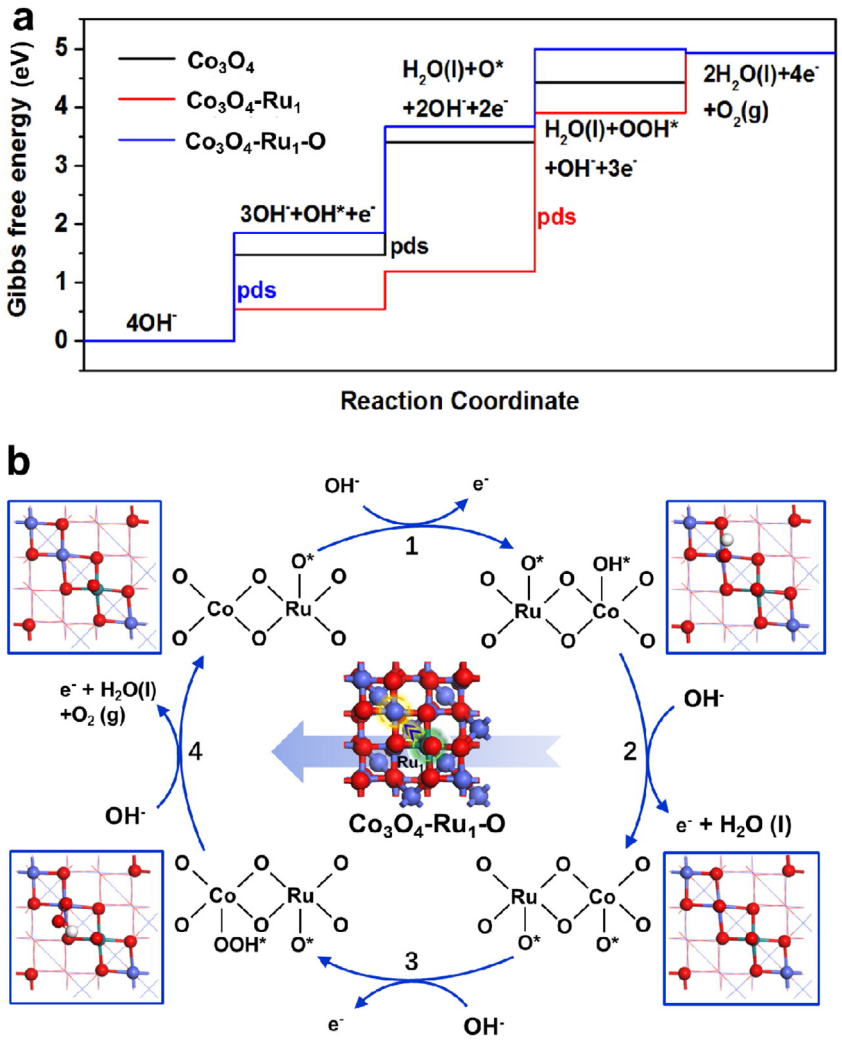

Fig. 4. DFT results of OER on various catalysts. (a) Free energy profiles of the intermediate states in OER on Co_3O_4 (001), Co_3O_4 (001)-Ru_1, and Co_3O_4 (001)-Ru_1-O surfaces at zero potential (U = 0 V). (b) Proposed reaction pathways of OER on Co_3O_4 (001)-Ru_1-O surface.

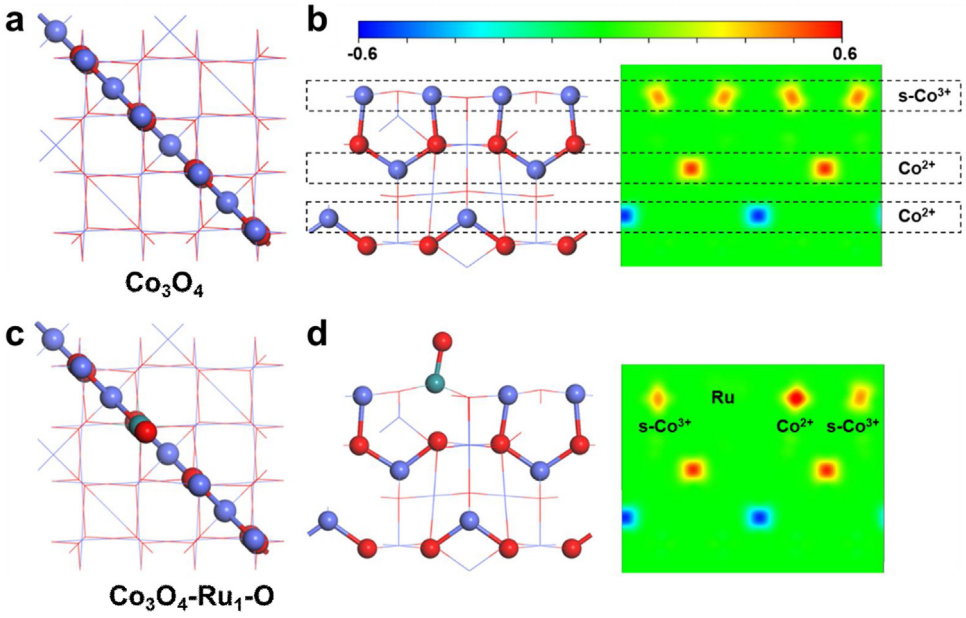

Fig. 5. The calculated spin density of (a, b) Co_3O_4 and (c, d) Co_3O_4-Ru_1-O surfaces. (a, c) are the top view and (b, d) are the side view. The balls in (a, c) represent the surface we cut to form 2D spin density figure in (b, d).

RuO_2 and Co_3O_4-Ru_1 are influenced by the oxidation peak of Ni foam substrate. After deducting the contribution of pure Co_3O_4, the Tafel slope of Co_3O_4-Ru_1 is 66 mV/decade which is lower than that of the Co_3O_4.

For further studying the enhanced catalytic activity, the electrochemically active surface areas of catalysts were investigated by using the electrochemical double-layer capacitance (Fig. S11). As shown in Fig. 3c, the Co_3O_4-Ru_1 exhibits significantly increased electrochemically active surface area of 154.4 mF cm^{-2} which is much higher than that of the pure Co_3O_4 (65.1 mF cm^{-2}), further indicating the increase of active sites after depositing single-atom Ru. For deep comparing the catalytic activity of the pure Co_3O_4 and Co_3O_4-Ru_1, the TOFs at different overpotentials were calculated (Fig. 3d). It can be noted that the TOF of Co_3O_4-Ru_1 is much higher than that of pure Co_3O_4. On the basis of the total Co atoms, the TOFs of pure Co_3O_4 and Co_3O_4-Ru_1 at 350 mV are 0.00088 s^{-1} and 0.013 s^{-1}, respectively, meaning that 13 times of activity was enhanced. Based on the surface Co atoms, the TOF of Co_3O_4 is also just 0.0063 s^{-1}. According to the deducted curve (Fig. 3a) and the activated Co sites (number of Ru atoms), the TOF of Co_3O_4-Ru_1 at 350 mV is 0.92 s^{-1}, which is 1043 times more than the pure Co_3O_4 (Fig. 3e). Compared with the surface Co atoms (the ratio of Co to Ru detected by XPS, Table S1), the catalytic activity of activated Co sites in Co_3O_4-Ru_1 is also 95.5 times as high as pure Co_3O_4.

More importantly, the as-prepared Co_3O_4-Ru_1 also exhibited long-term operation stability for over 100 h without obvious degradation. After the cycling test, there is no obvious Ru particle on the surface of Co_3O_4 (Fig. S12), and the ratio of surface Co to Ru is still 12.1 close to the 10.9 before testing (Table S1). These results reveal that Ru single atoms rarely aggregate and are barely dissolved under the electrochemical test, thus leading to excellent cycling stability. This is due to the strong interaction between single-atom Ru and the substrate of Co_3O_4. Comparing the electrochemical performance of this work with the works previously reported in the literature (Table S3), it is noted that the performance of Co_3O_4-Ru_1 is among the best performances of the Co_3O_4-based catalysts. For further comparison, the OER polarization curve of Co_3O_4-5Ru was also tested under the same conditions. As shown in Fig. S14, the catalyst of Co_3O_4-5Ru also shows improved catalytic activity in comparison to Co_3O_4, evidenced by the low overpotentials of 245 mV and 308 mV at 10 mA cm^{-2} and 50 mA cm^{-2}, respectively. This is also attributed to the deposition of a large amount of single-atom Ru.

In order to identify the effects of single-atom Ru on modulating the electronic structure of Co_3O_4 and the consequent OER reactivity, DFT calculations were performed. The (001) surface of Co_3O_4, featuring the best performance for OER, was chosen to study the interaction with single-atom Ru and catalytic activity. In an alkaline environment, the overall OER process could be described by the following four-step mechanism [46]:

$$\text{Step1}: OH^- + * \rightarrow OH* + e^-$$

$$\text{Step2}: OH^- + OH* \rightarrow O* + H_2O + e^-$$

$$\text{Step3}: OH^- + O* \rightarrow OOH* + e^-$$

$$\text{Step4}: OH^- + OOH* \rightarrow O_2 + H_2O + e^-$$

The free-energy profile of the OER process on Co_3O_4 (001)-Ru_1 is illustrated in the red line in Fig. 4a, and the optimized structures are shown in Fig. S15. The first step is the formation of *OH with the uphill free-energy profile of 0.54 eV. The formed *OH species absorbs on single-atom Ru surface rather than the surface of Co atoms, and *OH will further lose one proton with the endothermic ΔG of 0.65 eV. The third step with the formation of *OOH is the potential determining step (pds) in the OER process, where the ΔG is calculated to be as large as 2.71 eV. Hence, the theoretical overpotential (η) at standard conditions is 1.48 V, indicating the low OER activity of Co_3O_4 (001)-Ru_1 due to the strong binding energy of the catalyst with *O. We then consider the O covered surface (denoted as Co_3O_4 (001)-Ru_1-O). When Ru sites are covered by *O species, the *OH, *O, and *OOH species formed in the OER process all locate at the neighboring Co site, as shown in Fig. 4b. The free-energy profile of the OER process is illustrated in Fig. 4a and Fig. S16, and the calculation data are listed in Table S4. The weaker binding energy of *O on Co site reduce the free energy barrier of the third step (the formation of *OOH), and the first step determines the η in the whole OER process, which is calculated to be 0.62 V. For comparison, the free-energy profile of the OER process on Co_3O_4 (001) surface is also investigated as shown in Fig. 4a and Fig. S17. The calculation data are listed in Table S5. It is found the pds is the second step, where the *OH loses one proton to form *O with the endothermic energy of 1.94 eV (η = 0.71 V). Hence, we can conclude that although Ru single atoms are not the active sites for the oxygen evolution, the presence of Ru single atoms indeed enhances the OER activity of Co_3O_4 with reducing overpotential of ~0.1 V, which is consistent with the experimental results.

For further understanding the enhanced catalytic activity of the Co site adjacent to Ru atom, the spin densities of Co_3O_4 and Co_3O_4-Ru_1-O surfaces were calculated. As shown in Fig. 5, after introducing the Ru single atom with an O atom cover, the electronic configuration of surface Co atom is changed and reduced from Co^{3+} to Co^{2+}. The weaker binding energy of *O on Co site than on Ru site reduces the free energy barrier of the third step, changing the potential determining step and further decreasing the theoretical overpotential. In this case, Ru single atoms are not the real active sites, and the role is to adjust the electronic structure of adjacent Co atom and boost the catalytic activity.

Conclusion

In summary, we successfully developed a single-atom doping approach to activating the catalytic activity of inert Co_3O_4. The isolated Ru single atoms were uniformly deposited on the surface of Co_3O_4 by an advanced ALD method and confirmed by AC HAADF-STEM and XAS. As the catalyst for OER, the catalytic activity of Co_3O_4 was triggered and enhanced for as much as 95.5 times. In turn, a significantly lowered overpotential was achieved. The significantly enhanced catalytic activity is attributed to the effect of single-atom Ru on adjusting the electronic structure of adjacent Co atom, which results in an appropriate binding energy with oxygen-related intermediates. This study opens up a new avenue for the revelation of the new function of single atoms in modulating the surface electronic configuration and the design of catalyst with high catalytic activity.

CRediT authorship contribution statement

Changtai Zhao: Conceptualization, Methodology, Formal analysis, Investigation, Validation, Writing - original draft. **Yan Tang:** Formal analysis, Investigation, Writing - original draft. **Chang Yu:** Conceptualization, Formal analysis, Writing - review & editing. **Xinyi Tan:** Formal analysis, Validation. **Mohammad Norouzi Banis:** Methodology, Investigation. **Shaofeng Li:** Formal analysis. **Gang Wan:** Formal analysis. **Huawei Huang:** Formal analysis. **Lei Zhang:** Methodology. **Huaixin Yang:** Formal analysis. **Jun Li:** Conceptualization, Formal analysis, Supervision, Project administration. **Xueliang Sun:** Conceptualization, Supervision, Project administration. **Jieshan Qiu:** Conceptualization, Writing - review & editing, Funding acquisition, Supervision, Project administration.

Declaration of Competing Interest

The authors declare that they have no known competing financial interests or personal relationships that could have appeared to influence the work reported in this paper.

Acknowledgements

C. Zhao and Y. Tang contributed equally to this work. This work was partly supported by the National Natural Science Foundation of China (NSFC, Grant Nos. 21522601 and U1508201), the National Key Research and Development Program of China (Grant No. 2016YFB0101201), the Natural Sciences and Engineering Research Council of Canada (NSERC), the Canada Research Chair Program (CRC), the Canada Foundation for Innovation (CFI), and the Western University. The calculations were performed by using super-computers at Tsinghua National Laboratory for Information Science and Technology.

Appendix A. Supplementary data

Supplementary material related to this article can be found, in the online version, at doi:https://doi.org/10.1016/j.nantod.2020.100955.

References

[1] M.W. Kanan, D.G. Nocera, Science 321 (2008) 1072–1075.
[2] S. Chu, A. Majumdar, Nature 488 (2012) 294.
[3] J. Mao, C.-T. He, J. Pei, W. Chen, D. He, Y. He, Z. Zhuang, C. Chen, Q. Peng, D. Wang, Y. Li, Nat. Commun. 9 (2018) 4958.
[4] M.T.M. Koper, J. Electroanal. Chem. 660 (2011) 254–260.
[5] I.C. Man, H.-Y. Su, F. Calle-Vallejo, H.A. Hansen, J.I. Martínez, N.G. Inoglu, J. Kitchin, T.F. Jaramillo, J.K. Nørskov, J. Rossmeisl, ChemCatChem 3 (2011) 1159–1165.
[6] B.Y. Xia, Y. Yan, N. Li, H.B. Wu, X.W. Lou, X. Wang, Nat. Energy 1 (2016) 15006.
[7] J. Shan, C. Guo, Y. Zhu, S. Chen, L. Song, M. Jaroniec, Y. Zheng, S.-Z. Qiao, Chem 5 (2019) 445–459.
[8] T.Y. Ma, S. Dai, M. Jaroniec, S.Z. Qiao, J. Am. Chem. Soc. 136 (2014) 13925–13931.
[9] J. Bao, X. Zhang, B. Fan, J. Zhang, M. Zhou, W. Yang, X. Hu, H. Wang, B. Pan, Y. Xie, Angew. Chem. Int. Ed. 54 (2015) 7399–7404.
[10] Z.-W. Gao, J.-Y. Liu, X.-M. Chen, X.-L. Zheng, J. Mao, H. Liu, T. Ma, L. Li, W.-C. Wang, X.-W. Du,Adv. Mater. 31 (2019), 1804769.
[11] Y. Wang, T. Zhou, K. Jiang, P. Da, Z. Peng, J. Tang, B. Kong, W.-B. Cai, Z. Yang, G. Zheng,Adv. Energy Mater. 4 (2014), 1400696.
[12] S. Zhao, Y. Wang, J. Dong, C.-T. He, H. Yin, P. An, K. Zhao, X. Zhang, C. Gao, L. Zhang, J. Lv, J. Wang, J. Zhang, A.M. Khattak, N.A. Khan, Z. Wei, J. Zhang, S. Liu, H. Zhao, Z. Tang, Nat. Energy 1 (2016) 16184.
[13] F. Song, X. Hu, Nat. Commun. 5 (2014) 4477.
[14] X. Lu, C. Zhao, Nat. Commun. 6 (2015) 6616.
[15] C. Zhao, C. Yu, H. Huang, X. Han, Z. Liu, J. Qiu, Energy Storage Mater. 10 (2018) 291–296.
[16] L. Xie, R. Zhang, L. Cui, D. Liu, S. Hao, Y. Ma, G. Du, A.M. Asiri, X. Sun, Angew. Chem. Int. Ed. 56 (2017) 1064–1068.
[17] J.K. Nørskov, F. Abild-Pedersen, F. Studt, T. Bligaard, Proc. Natl. Acad. Sci. U. S. A. 108 (2011) 937–943.
[18] Y. Yao, S. Hu, W. Chen, Z.-Q. Huang, W. Wei, T. Yao, R. Liu, K. Zang, X. Wang, G. Wu, W. Yuan, T. Yuan, B. Zhu, W. Liu, Z. Li, D. He, Z. Xue, Y. Wang, X. Zheng, J. Dong, C.-R. Chang, Y. Chen, X. Hong, J. Luo, S. Wei, W.-X. Li, P. Strasser, Y. Wu, Y. Li, Nat. Catal. 2 (2019) 304–313.
[19] T. Tang, W.-J. Jiang, S. Niu, N. Liu, H. Luo, Y.-Y. Chen, S.-F. Jin, F. Gao, L.-J. Wan, J.-S. Hu, J. Am. Chem. Soc. 139 (2017) 8320–8328.
[20] X. Long, J. Li, S. Xiao, K. Yan, Z. Wang, H. Chen, S. Yang, Angew. Chem. Int. Ed. 53 (2014) 7584–7588.
[21] C.C.L. McCrory, S. Jung, J.C. Peters, T.F. Jaramillo, J. Am. Chem. Soc. 135 (2013) 16977–16987.
[22] P. Liao, J.A. Keith, E.A. Carter, J. Am. Chem. Soc. 134 (2012) 13296–13309.
[23] M. Bajdich, M. García-Mota, A. Vojvodic, J.K. Nørskov, A.T. Bell, J. Am. Chem. Soc. 135 (2013) 13521–13530.
[24] J.O.M. Bockris, T. Otagawa, J. Electrochem. Soc. 131 (1984) 290–302.
[25] J. Suntivich, K.J. May, H.A. Gasteiger, J.B. Goodenough, Y. Shao-Horn, Science 334 (2011) 1383–1385.
[26] B. Zhang, X. Zheng, O. Voznyy, R. Comin, M. Bajdich, M. García-Melchor, L. Han, J. Xu, M. Liu, L. Zheng, F.P. García de Arquer, C.T. Dinh, F. Fan, M. Yuan, E. Yassitepe, N. Chen, T. Regier, P. Liu, Y. Li, P. De Luna, A. Janmohamed, H.L. Xin, H. Yang, A. Vojvodic, E.H. Sargent, Science 352 (2016) 333–337.
[27] A. Wang, J. Li, T. Zhang, Nat. Rev. Chem. 2 (2018) 65–81.
[28] B. Qiao, A. Wang, X. Yang, L.F. Allard, Z. Jiang, Y. Cui, J. Liu, J. Li, T. Zhang, Nat. Chem. 3 (2011) 634.
[29] D. Wang, Q. Li, C. Han, Z. Xing, X. Yang, Appl. Catal. B: Environ. 249 (2019) 91–97.
[30] J. Zhang, C. Liu, B. Zhang,Small Methods 3 (2019), 1800481.
[31] H. Fei, J. Dong, M.J. Arellano-Jiménez, G. Ye, N. Dong Kim, E.L.G. Samuel, Z. Peng, Z. Zhu, F. Qin, J. Bao, M.J. Yacaman, P.M. Ajayan, D. Chen, J.M. Tour, Nat. Commun. 6 (2015) 8668.
[32] Y. Chen, S. Ji, C. Chen, Q. Peng, D. Wang, Y. Li, Joule 2 (2018) 1242–1264.
[33] P. Li, M. Wang, X. Duan, L. Zheng, X. Cheng, Y. Zhang, Y. Kuang, Y. Li, Q. Ma, Z. Feng, W. Liu, X. Sun, Nat. Commun. 10 (2019) 1711.
[34] J. Deng, H. Li, J. Xiao, Y. Tu, D. Deng, H. Yang, H. Tian, J. Li, P. Ren, X. Bao, Energy Environ. Sci. 8 (2015) 1594–1601.
[35] Z. Luo, Y. Ouyang, H. Zhang, M. Xiao, J. Ge, Z. Jiang, J. Wang, D. Tang, X. Cao, C. Liu, W. Xing, Nat. Commun. 9 (2018) 2120.
[36] J. Zhang, J. Liu, L. Xi, Y. Yu, N. Chen, S. Sun, W. Wang, K.M. Lange, B. Zhang, J. Am. Chem. Soc. 140 (2018) 3876–3879.
[37] G. Kresse, J. Furthmüller, Phys. Rev. B 54 (1996) 11169–11186.
[38] G. Kresse, J. Furthmüller, Comput. Mater. Sci. 6 (1996) 15–50.
[39] G. Kresse, D. Joubert, Phys. Rev. B 59 (1999) 1758–1775.
[40] J.P. Perdew, K. Burke, M. Ernzerhof, Phys. Rev. Lett. 77 (1996) 3865–3868.
[41] S.L. Dudarev, G.A. Botton, S.Y. Savrasov, C.J. Humphreys, A.P. Sutton, Phys. Rev. B 57 (1998) 1505–1509.
[42] V.I. Anisimov, F. Aryasetiawan, A.I. Lichtenstein, J. Phys. Condens. Matter 9 (1997) 767–808.
[43] S. Selcuk, A. Selloni, J. Phys. Chem. C 119 (2015) 9973–9979.
[44] N. Cheng, S. Stambula, D. Wang, M.N. Banis, J. Liu, A. Riese, B. Xiao, R. Li, T.-K. Sham, L.-M. Liu, G.A. Botton, X. Sun, Nat. Commun. 7 (2016) 13638.
[45] A. Bergmann, E. Martinez-Moreno, D. Teschner, P. Chernev, M. Gliech, J.F. de Araújo, T. Reier, H. Dau, P. Strasser, Nat. Commun. 6 (2015) 8625.
[46] J. Rossmeisl, Z.W. Qu, H. Zhu, G.J. Kroes, J.K. Nørskov, J. Electroanal. Chem. 607 (2007) 83–89.